

Assessing the reliability of the MODIS LST product to detect temporal variability

Shuo Xu^a, Dongdong Wang^{a*}, Shunlin Liang^a, Yunyue Yu^b, Yuling Liu^c, Aolin Jia^a

^a Department of Geographical Sciences, University of Maryland, College Park, MD, 20742, USA

^b NOAA NESDIS Center for Satellite Applications and Research, College Park, MD 20740,
USA

^c Earth System Science Interdisciplinary Center, University of Maryland, College Park, MD
20740, USA

*Corresponding author:

Dongdong Wang

Department of Geographical Sciences, University of Maryland, College Park, MD, 20742, USA.

E-mail address: ddwang@umd.edu

Xu, Shuo, Dongdong Wang, Shunlin Liang, Yuling Liu and Aolin Jia, Assessing the reliability of the MODIS LST product to detect temporal variability, IEEE Geosci. Remote Sens. Lett., **20**(9), 2504505, <https://dx.doi.org/10.1109/LGRS.2023.3312384>.

Abstract

Land surface temperature (LST) data acquired from satellites are used extensively in studying climate variability. Many researchers have used Moderate Resolution Imaging Spectroradiometer (MODIS) LST to detect the temperature trend, however, its reliability has not been fully investigated. Using in-situ data acquired from 67 stations worldwide, this study examined the reliability of the detected temperature trends and investigated the associated influencing factors. The high-quality MODIS data have an RMSE of 2.44 K and 3.70 K at nighttime and daytime, respectively. However, its trend detection had an RMSE of 0.81 K/decade and 0.98 K/decade at nighttime and daytime, respectively. Clear-sky bias, quality control, LST estimation uncertainties, trend magnitude, and length of time were factors that influenced the detected trends. Filling cloud-covered areas in MODIS data may effectively reduce biases in trend detection.

Index Terms—temperature, trend, MODIS, in-situ measurements.

I. INTRODUCTION

As reported by the Intergovernmental Panel on Climate Change (IPCC), global average temperatures have risen by approximately 1.5 °C since the pre-industrial era [1]. However, climate variability research typically relies on near-surface air temperature data, which are conventionally obtained from meteorological stations, buoy observations, and climate models. These data sources represent sparsely distributed data or simulated values.

Land surface temperature (LST) is an important parameter for measuring the energy balance at the Earth's surface, which is related to climatic variability [2]. In the past, the lack of long-term LST records has hindered the application of satellite LST in climate studies, and only a few studies have examined the role of LST datasets in climate variations [3, 4]. However, with the development of remote sensing technology, long-term, large-scale, and high-density LST data can be retrieved from satellites [5-7], which can help in studying climate variability.

Among satellite products, the Moderate Resolution Imaging Spectroradiometer (MODIS) LST is commonly used, with previous studies reporting a root mean square error (RMSE) value of 0.75-5.58 K under different scenarios [8]. While many researchers have used MODIS LST products to investigate temperature trends [9-11], only a few have evaluated the reliability of these trends.

Sobrino, et al. [12] found MODIS LST trends at the global scale are very similar to the NOAA's National Climatic Data Center (NOAA-NCDC) air temperature dataset. However, these aggregated values on global or regional scales may mask the underlying complexities at finer scales, and it is challenging to precisely identify the exact values at global or regional scales. In contrast, station-scale data have the highest accuracy and are often considered to be the closest approximation to the true value. Therefore, assessing the reliability of MODIS LST trends at the station scale plays a key role in identifying sources of error in trend detection, improving the precision of detected trends, and developing strategies for improve existing datasets.

Therefore, in-situ data were collected from global field stations with multiple surface types and climatic zones to detect the actual multi-year temperature variability and investigate the reliability of satellite LST in predicting long-term temperature trends. Furthermore, the influencing factors of trends were explored.

II. SITES AND DATA

A. Selected Validation Sites

This study used surface upwelling longwave radiation (LWUP) and downward longwave radiation (LWDN) records to calculate in-situ LST and considered 67 sites that met the criteria of having records for more than ten years and MODIS LST data available. The 67 sites were selected from Surface Radiation Budget Network (SURFRAD) (7) (<https://gml.noaa.gov/grad/surfrad/>) [13, 14], Baseline Surface Radiation Network (BSRN) (10) (<https://bsrn.awi.de/>) [16], FLUXNET (10) (<https://fluxnet.org/data/>) [15], and AmeriFlux network (40) (<https://ameriflux.lbl.gov/>) [16], providing high-quality LWUP and LWDN measurements with a temporal resolution of 1-3 min, 1-60 min, 30 min, and 30 min, respectively. The majority of our data is within the 1-30 min range, and the maximum time difference between MODIS LST and in-situ measurements was 15 mins. Geolocation of these stations is shown in Fig. 1.

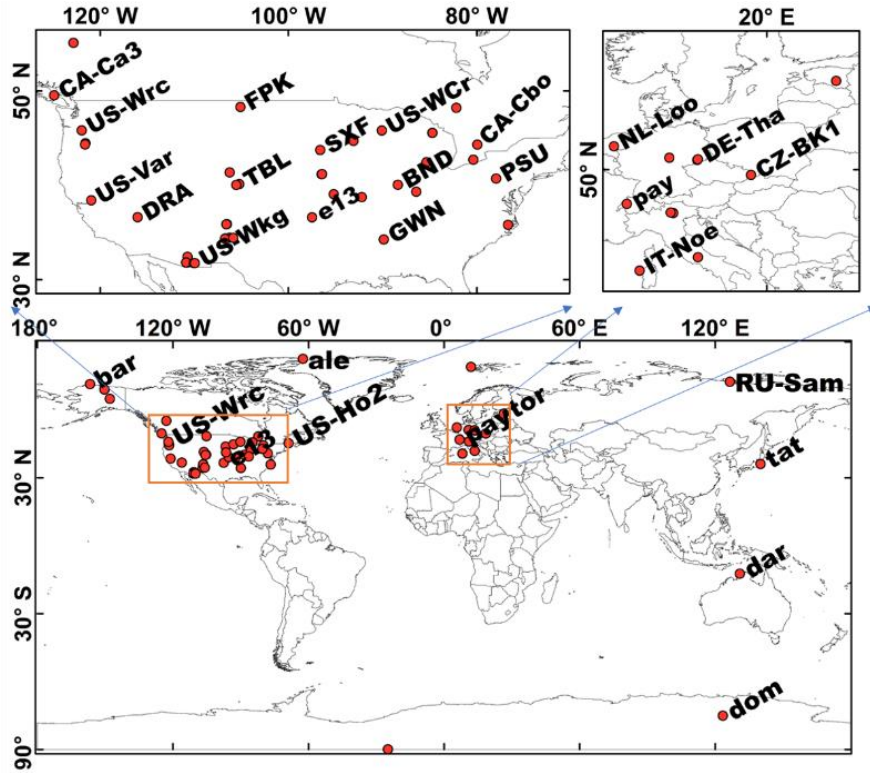


Fig. 1. Geolocation of stations.

B. MODIS LST Products

MODIS instruments on Terra and Aqua satellites provided daytime/nighttime LST observations at approximately 10:30 AM/PM and 1:30 AM/PM local time. We used National Aeronautics and Space Administration (NASA)'s Application for Extracting and Exploring Analysis Ready Samples (AppEARS) tool (<https://appears.earthdatacloud.nasa.gov/>) [17] to download and process the commonly used daily level-3 1-km MOD11A1 LST product (Version 006) for the study period from January 1, 2003, to December 31, 2020.

The LST, QC, and view time layers from the daily LST products were used. LST data were generated by the split-window technique [18, 19]. The QC information was used to identify clear/cloudy conditions: since thermal infrared (TIR) radiation cannot penetrate clouds to obtain LST data under the clouds, a clear sky was defined when the MODIS pixels were valid values,

while other cases were defined as a cloudy sky. Furthermore, the QC information was used to identify data quality: pixels labeled “LST produced, good quality, not necessary to examine more detailed QA” were selected as high-quality (HQ) data, while other pixels with valid values were identified as low-quality data. Additionally, the view time information from the daily LST products was used to match the in-situ data.

C. In-situ Measurements

The in-situ LST was calculated using LWUP and LWDN based on Stefan-Boltzmann theory as follows:

$$T_s = \left[\frac{F^\uparrow - (1 - \varepsilon_b)F^\downarrow}{\sigma \varepsilon_b} \right]^{1/4} \quad (1)$$

where T_s is the LST, F^\uparrow and F^\downarrow are LWUP and LWDN, respectively, ε_b is the surface broadband emissivity (BBE), and σ is the Stefan-Boltzmann constant ($5.67 \times 10^{-8} \text{ Wm}^{-2}\text{K}^{-4}$). Here, ε_b was obtained from the 8-day GLASS BBE product (<http://www.glass.umd.edu/BBE/AVHRR/>) [20, 21], and algorithm details are available at <http://www.glass.umd.edu/introduction.html>. The in-situ data that corresponded to all MODIS LST and HQ MODIS LST were designated as the clear-sky in-situ data and HQ in-situ data, respectively.

III. RESULTS

In this study, trends were determined in the form of least square line fitting, and the decade trend was used. We focused on HQ MODIS data since LST trends are mostly calculated using HQ MODIS data [9-11].

To assess the accuracy of HQ MODIS data, we compared it to in-situ measurements with a time difference less than half the in-situ data’s temporal resolution. We calculated RMSE separately for daytime and nighttime data:

$$\text{RMSE} = \sqrt{\frac{\sum_{i=1}^N (\hat{x}_i - x_i)^2}{N}} \quad (2)$$

where i represents variable i , \hat{x}_i represents the HQ MODIS time series, x_i represents the in-situ measurements time series, and N represents the total number of available data points.

Nighttime and daytime HQ MODIS LST data have RMSEs of 2.44 K and 3.70 K (Fig. 2(a)), which are comparable to the RMSEs of 0.75-5.58 K in a previous study [8].

For trend analysis, we compared the trends derived from HQ MODIS data with those from all-sky in-situ measurements. Table 1 presents the average values and standard deviations (STDs) of all trends. The RMSE for trend detection was computed separately for daytime and nighttime data:

$$\text{RMSE} = \sqrt{\frac{\sum_{i=1}^M (\hat{y}_i - y_i)^2}{M}} \quad (3)$$

where i represents variable i , \hat{y}_i represents the trend calculated from HQ MODIS data series, y_i represents the trend calculated from all-sky in-situ measurements series, and M represents the total number of available data points.

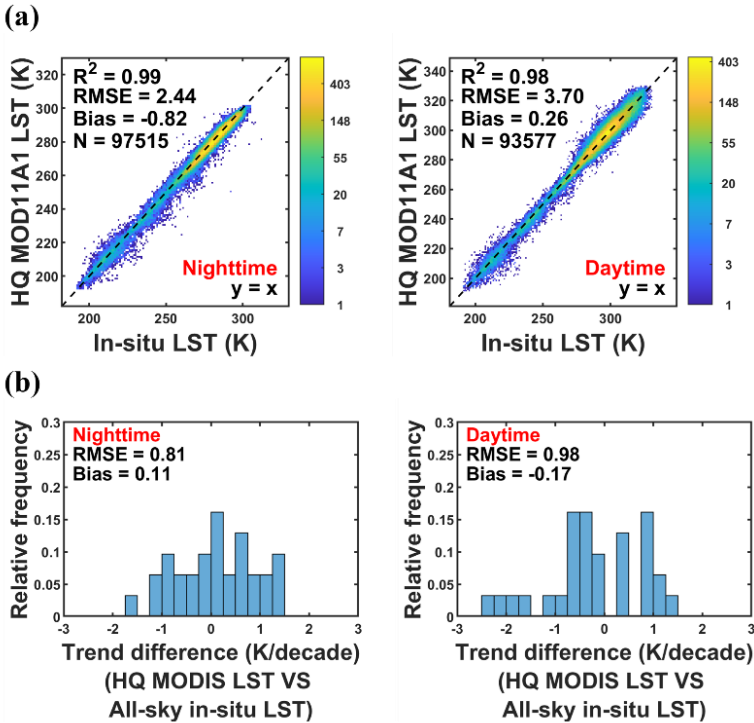


Fig. 2. Data comparison. (a) Comparison of high-quality (HQ) MODIS LST and in-situ LST; and (b) Trend differences between HQ MODIS LST and all-sky in-situ LST.

The trends of nighttime and daytime HQ MODIS LST have RMSEs of 0.81 K/decade and 0.98 K/decade compared with all-sky in-situ LST trends (Fig. 2(b)). This indicates that the trend detected from HQ MODIS LST may differ from the actual all-weather LST trend. We explored the factors that influence trends in the next section.

Table 1. The means and standard deviations (STDs) of the trends.

Trends (K/decade)	Nighttime		Daytime	
	Mean	STD	Mean	STD
HQ MODIS LST	0.37	0.53	0.14	0.66
All-sky in-situ LST	0.26	0.63	0.31	0.82
Clear-sky in-situ LST	0.28	0.64	0.28	0.84
MODIS LST	0.36	0.46	0.12	0.61

IV. DISCUSSION

We explored various influencing factors that may affect the accuracy of LST trends, including clear-sky bias of data, QC procedure, trend magnitude, LST error, and data length. To assess the effects of the clear-sky bias and the QC procedure on the calculated trends, we used in-situ LST data. For other factors, we utilized simulated data.

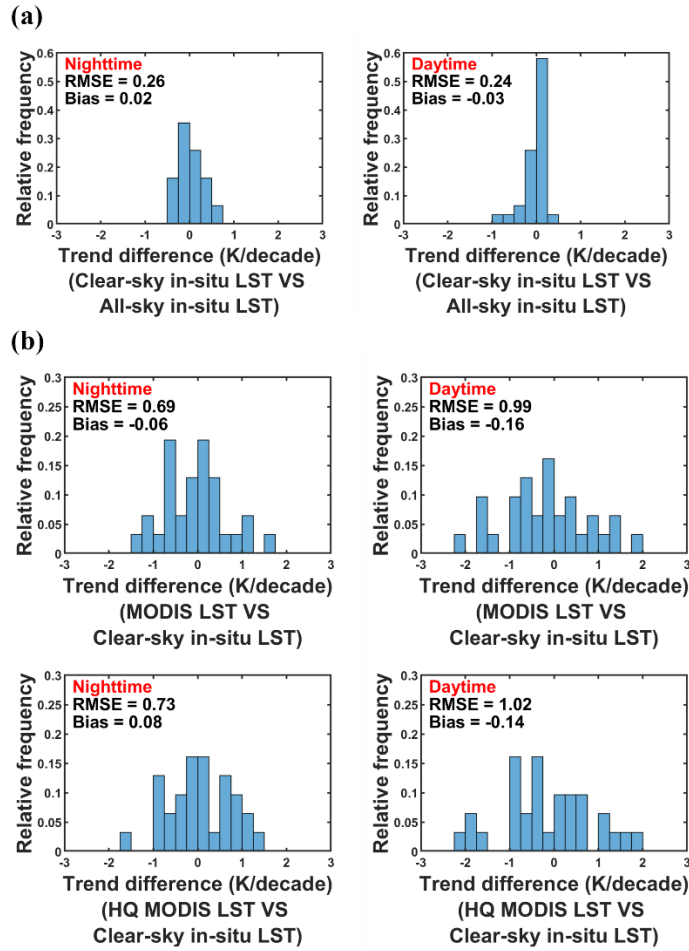


Fig. 3. Trend comparison. (a) Trend difference between clear-sky in-situ LST and all-sky in-situ LST; and (b) Trend difference between MODIS LST/ high-quality (HQ) MODIS LST and clear-sky in-situ LST.

A. Clear-sky Bias

One factor that can impact the accuracy of LST trends is the clear-sky bias. MODIS, as a TIR sensor, can only measure data under clear-sky conditions, which may not be representative of the climatological mean states and may exhibit clear-sky bias issues [22]. Clear-sky bias refers to the difference between clear-sky LSTs and all-weather LSTs [23]. In this study, we discussed the effects of clear-sky bias on the accuracy of LST trends using in-situ data.

The trends of nighttime and daytime clear-sky in-situ LSTs showed RMSEs of 0.26 K/decade and 0.24 K/decade, respectively, when compared with the trends detected by the all-sky in-situ LSTs (Fig. 3(a)). This indicates that the clear-sky bias of data led to errors in calculated LST trends.

B. Quality Control

Previous studies have utilized HQ MODIS data selected through the QC procedure [9-11], which may influence the detected trends. In this section, the effects of the QC procedure on the accuracy of LST trends have been discussed.

To distinguish the impacts of the QC procedure from the impacts of the clear-sky bias, we compared the trends detected by clear-sky in-situ data with those detected by HQ MODIS data.

Compared with the trends detected by clear-sky in-situ LSTs, the trends of nighttime and daytime MODIS LSTs exhibited RMSEs of 0.69 K/decade and 0.99 K/decade, respectively (The first row in Fig. 3(b)). In contrast, the trends of nighttime and daytime HQ MODIS LSTs showed RMSEs of 0.73 K/decade and 1.02 K/decade, respectively (The second row in Fig. 3(b)). This indicates that the accuracy of the trends detected by MODIS LSTs was slightly higher than the accuracy of the trends detected by HQ MODIS LSTs (0.04 K/decade and 0.03 K/decade for nighttime and daytime, respectively). Therefore, the QC procedure also contributed to errors in calculated LST trends.

One possible reason for this observation is that the QC procedure misses a significant amount of available data. After the QC procedure, the ratio of available daytime and nighttime MODIS LSTs was reduced by 44.30% and 39.9%, respectively.

C. LST Error

We explored the impact of LST error on the calculated trends using a simulation experiment that isolated its effects from clear-sky bias and QC procedure. We assumed that the LST and its errors

are normally distributed. While assuming a uniform error distribution simplifies some aspects of data analysis, it's essential to recognize that it may oversimplify the complexity of error patterns and may not adequately represent the behavior of errors during extreme events.

We generated error-free simulated data by setting mean (282.52 K), STD (9.73 K), and trend (0.94 K/decade) based on all-sky in-situ LST data, and then generated simulated data with errors by adding error arrays with the mean (0 K) and STD (0 K to 10 K, in 0.25 K intervals). For each LST error, we randomly generated 10,000 error arrays. The trend of the simulated data with and without errors was calculated. Their RMSE, percentage of trends with different signs, and percentage of trend difference were shown in Fig. 4(a).

The RMSE between error-free and error-containing data increased with increasing LST errors, reaching about 0.35 K/decade and 0.50 K/decade when the LST error was 2.44 K and 3.75 K (the RMSE of nighttime and daytime HQ MODIS LST). Moreover, the percentage of the trend for different signs increased with increasing LST errors starting from an LST error of about 2.50 K. These results indicated that the LST error contributed to the error in detected trends, and as the LST error increased, the accuracy of the trend decreased.

D. Trend Magnitude

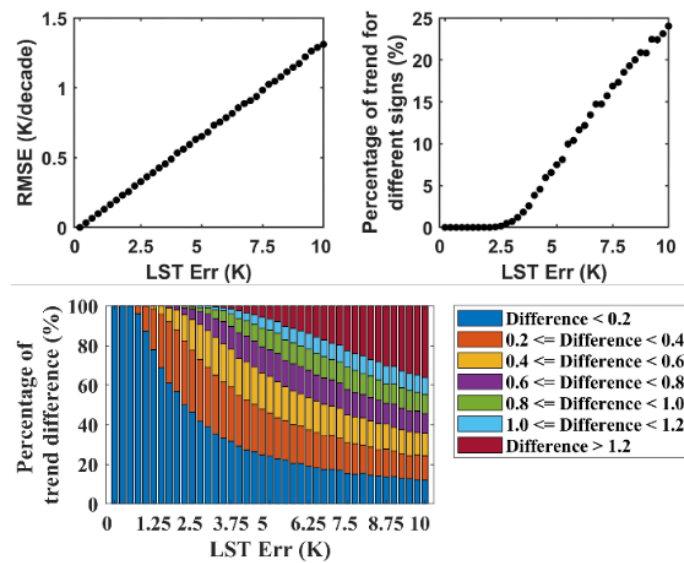
We investigated the error tolerance on arrays with different trend magnitudes by introducing the same errors. We generated simulated data with fixed trend magnitudes ranging from -1.50 K/decade to 1.50 K/decade, and then generated simulated data with errors by adding error arrays with STD of 2.50 K. In this process, 10,000 error arrays were generated. The trend of the simulated data with and without error was calculated. Their RMSE, percentage of trends with different signs, and percentage of trend difference were shown in Fig. 4(b).

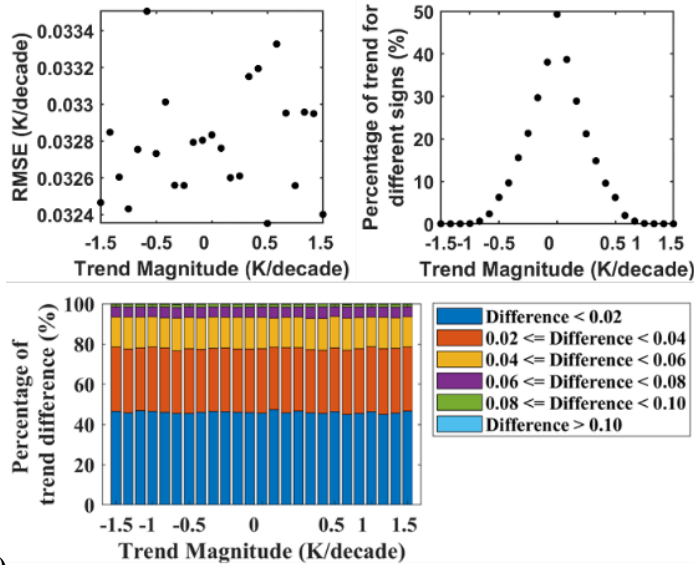
The RMSE showed a random variation with the trend magnitude, and the percentage of trends

with different signs decreased as the absolute value of the trend magnitude increased until an absolute value of 1.00 K/decade was reached. Additionally, the percentage of trend difference was almost constant for different trend magnitudes. Therefore, error tolerance is weaker for smaller trend magnitudes, and large trend magnitudes in the data make it easier to maintain the sign of the trend.

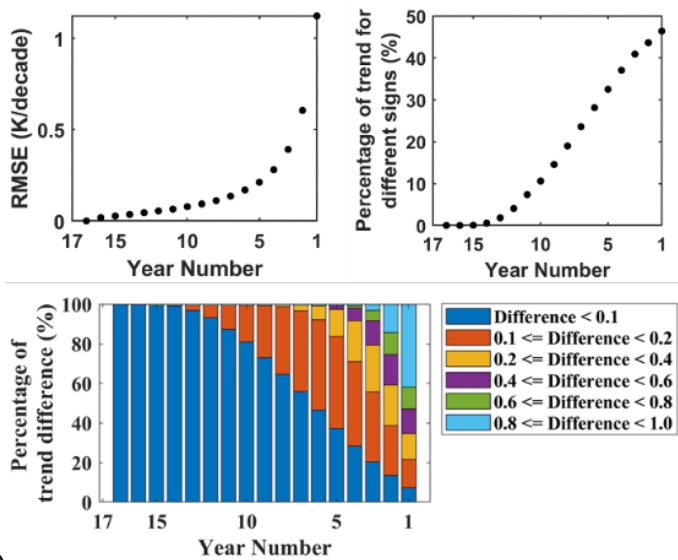
E. Length of Time

(a)





(b)



(c)

Fig 4. The statistical matrix of errors caused by: (a) LST errors (LST Err); (b) Trend magnitude; (c) Year number.

To explore the effect of time on temperature trends, 10,000 complete 17-year simulated datasets were randomly generated by setting their mean (282.52 K), STD (9.73 K), and trend (0.94 K/decade). To obtain shorter time periods, some data at the beginning of the matrix were

subtracted. Temperature trends were computed for both the 17-year and shorter time periods, and their RMSE, percentage of trends with different signs, and percentage of trend difference were depicted in Fig. 4(c).

The RMSE increased with decreasing number of years and the RMSE was < 0.10 K/decade when the data length was > 10 years. The percentage of the trend for different signs increased with decreasing number of years starting from 14 years. Additionally, a trend difference of > 0.10 K/decade was observed when the data length was < 15 years. The results indicated that a decrease in the time period led to a decrease in trend accuracy.

V. CONCLUSION

This study evaluated the reliability of long-term, large-scale, high-density spatially sampled MODIS data in capturing the temporal variability of LST, using in-situ data collected from 67 stations worldwide with multiple surface types and climatic zones.

The HQ MODIS data showed high accuracy, with nighttime and daytime RMSE values of 2.44 K and 3.70 K, respectively. However, its trend was not sufficiently accurate to indicate multi-year variations in actual all-sky LSTs, with nighttime and daytime RMSE values of 0.81 K/decade and 0.98 K/decade, respectively.

The study also identified several factors that affected the detected trends: 1) The clear-sky bias led to an RMSE of 0.26 K/decade and 0.24 K/decade for the nighttime and daytime trends, respectively. 2) The QC procedure led to an RMSE of 0.04 K/decade and 0.03 K/decade RMSE for the nighttime and daytime trends, respectively. 3) The LST error led to an RMSE of 0.35 K/decade and 0.50 K/decade for the nighttime and daytime trends, respectively. 4) Larger trend magnitudes in the data made it easier to maintain the sign of the trend. 5) When the data length was less than 15 years, a trend difference greater than 0.10 K/decade was observed. This analysis

will help users understand the sources of errors in detecting trends using MODIS LST data. By understanding these sources of error, users can make more informed decisions about how to use MODIS LST data for trend analysis. For instance, they can employ established fusion methods [6, 24-26] to effectively fill cloud-covered areas in MODIS data, thereby reducing biases in trend detection effectively.

However, despite our efforts to choose in-situ LST data that closely match with MODIS data in time, in-situ measurements with higher temporal resolutions are still limited. In future studies, we will incorporate more in-situ data with higher temporal resolution to improve accuracy.

ACKNOWLEDGEMENT

Shuo Xu, Dongdong Wang, and Yuling Liu were funded by NOAA grant NA19NES4320002 (COOPERATIVE INSTITUTE FOR SATELLITE EARTH SYSTEM STUDIES, CISESS).

REFERENCES

- [1] V. Masson-Delmotte, P. Zhai, H.-O. Pörtner, D. Roberts, J. Skea, and P. R. Shukla, Global Warming of 1.5 C: IPCC special report on impacts of global warming of 1.5 C above pre-industrial levels in context of strengthening response to climate change, sustainable development, and efforts to eradicate poverty. Cambridge University Press, 2022.
- [2] S. Xu, J. Cheng, and Q. Zhang, "A Random Forest-Based Data Fusion Method for Obtaining All-Weather Land Surface Temperature with High Spatial Resolution," Remote Sensing, vol. 13, no. 11, p. 2211, 2021. [Online]. Available: <https://www.mdpi.com/2072-4292/13/11/2211>.

- [3] J. C. Jiménez-Muñoz, J. A. Sobrino, C. Mattar, and Y. Malhi, "Spatial and temporal patterns of the recent warming of the Amazon forest," *Journal of Geophysical Research: Atmospheres*, vol. 118, no. 11, pp. 5204-5215, 2013.
- [4] I. F. Trigo, I. T. Monteiro, F. Olesen, and E. Kabsch, "An assessment of remotely sensed land surface temperature," *Journal of Geophysical Research: Atmospheres*, vol. 113, no. D17, 2008.
- [5] Z.-L. Li et al., "Satellite-derived land surface temperature: Current status and perspectives," *Remote sensing of environment*, vol. 131, pp. 14-37, 2013.
- [6] A. Jia, S. Liang, D. Wang, L. Ma, Z. Wang, and S. Xu, "Global hourly, 5 km, all-sky land surface temperature data from 2011 to 2021 based on integrating geostationary and polar-orbiting satellite data," *Earth Syst. Sci. Data Discuss.*, vol. 2022, pp. 1-35, 2022, doi: 10.5194/essd-2022-284.
- [7] Q. Zhang, N. Wang, J. Cheng, and S. Xu, "A Stepwise Downscaling Method for Generating High-Resolution Land Surface Temperature From AMSR-E Data," *IEEE Journal of Selected Topics in Applied Earth Observations and Remote Sensing*, vol. 13, pp. 5669-5681, 2020, doi: 10.1109/JSTARS.2020.3022997.
- [8] S.-B. Duan et al., "Validation of Collection 6 MODIS land surface temperature product using in situ measurements," *Remote sensing of environment*, vol. 225, pp. 16-29, 2019.
- [9] D. Eleftheriou et al., "Determination of annual and seasonal daytime and nighttime trends of MODIS LST over Greece - climate change implications," *Science of The Total Environment*, vol. 616-617, pp. 937-947, 2018/03/01/ 2018, doi: <https://doi.org/10.1016/j.scitotenv.2017.10.226>.
- [10] A. Polydoros, T. Mavrakou, and C. Cartalis, "Quantifying the Trends in Land Surface Temperature and Surface Urban Heat Island Intensity in Mediterranean Cities in View of Smart

Urbanization," *Urban Science*, vol. 2, no. 1, p. 16, 2018. [Online]. Available: <https://www.mdpi.com/2413-8851/2/1/16>.

[11] W. Zhao, J. He, Y. Wu, D. Xiong, F. Wen, and A. Li, "An Analysis of Land Surface Temperature Trends in the Central Himalayan Region Based on MODIS Products," *Remote Sensing*, vol. 11, no. 8, p. 900, 2019. [Online]. Available: <https://www.mdpi.com/2072-4292/11/8/900>.

[12] J. A. Sobrino, S. García-Monteiro, and Y. Julien, "Surface Temperature of the Planet Earth from Satellite Data over the Period 2003–2019," *Remote Sensing*, vol. 12, no. 12, p. 2036, 2020. [Online]. Available: <https://www.mdpi.com/2072-4292/12/12/2036>.

[13] J. A. Augustine, J. J. DeLuisi, and C. N. Long, "SURFRAD—A national surface radiation budget network for atmospheric research," *Bulletin of the American Meteorological Society*, vol. 81, no. 10, pp. 2341-2358, 2000.

[14] J. A. Augustine, G. B. Hodges, C. R. Cornwall, J. J. Michalsky, and C. I. Medina, "An update on SURFRAD—The GCOS surface radiation budget network for the continental United States," *Journal of Atmospheric and Oceanic Technology*, vol. 22, no. 10, pp. 1460-1472, 2005.

[15] G. Pastorello et al., "The FLUXNET2015 dataset and the ONEFlux processing pipeline for eddy covariance data," *Sci Data*, vol. 7, no. 1, p. 225, 2020/07/09 2020, doi: 10.1038/s41597-020-0534-3.

[16] W. W. Hargrove, F. M. Hoffman, and B. E. Law, "New analysis reveals representativeness of the AmeriFlux network," *Eos, Transactions American Geophysical Union*, vol. 84, no. 48, pp. 529-535, 2003.

- [17] A. Team, "Application for extracting and exploring analysis ready samples (AppEEARS)," USGS/Earth Resources Observation and Science (EROS) Center, Sioux Falls, South Dakota, USA, 2019.
- [18] Z. Wan, "New refinements and validation of the collection-6 MODIS land-surface temperature/emissivity product," *Remote sensing of Environment*, vol. 140, pp. 36-45, 2014.
- [19] Z. Wan and J. Dozier, "A generalized split-window algorithm for retrieving land-surface temperature from space," *IEEE Transactions on geoscience and remote sensing*, vol. 34, no. 4, pp. 892-905, 1996.
- [20] J. Cheng and S. Liang, "Estimating the broadband longwave emissivity of global bare soil from the MODIS shortwave albedo product," *Journal of Geophysical Research: Atmospheres*, vol. 119, no. 2, pp. 614-634, 2014.
- [21] J. Cheng, S. Liang, W. Verhoef, L. Shi, and Q. Liu, "Estimating the hemispherical broadband longwave emissivity of global vegetated surfaces using a radiative transfer model," *IEEE Transactions on Geoscience and Remote Sensing*, vol. 54, no. 2, pp. 905-917, 2015.
- [22] T. Chakraborty, A. Hsu, D. Manya, and G. Sheriff, "A spatially explicit surface urban heat island database for the United States: Characterization, uncertainties, and possible applications," *ISPRS Journal of Photogrammetry and Remote Sensing*, vol. 168, pp. 74-88, 2020.
- [23] S. L. Ermida, I. F. Trigo, C. C. DaCamara, C. Jiménez, and C. Prigent, "Quantifying the Clear-Sky Bias of Satellite Land Surface Temperature Using Microwave-Based Estimates," *Journal of Geophysical Research: Atmospheres*, vol. 124, no. 2, pp. 844-857, 2019, doi: <https://doi.org/10.1029/2018JD029354>.
- [24] S. Xu, J. Cheng, and Q. Zhang, "Reconstructing All-Weather Land Surface Temperature Using the Bayesian Maximum Entropy Method Over the Tibetan Plateau and Heihe River Basin,"

IEEE Journal of Selected Topics in Applied Earth Observations and Remote Sensing, vol. 12, no. 9, pp. 3307-3316, 2019, doi: 10.1109/JSTARS.2019.2921924.

[25] S. Xu and J. Cheng, "A new land surface temperature fusion strategy based on cumulative distribution function matching and multiresolution Kalman filtering," Remote Sensing of Environment, vol. 254, p. 112256, 2021.

[26] S. Xu, D. Wang, S. Liang, Y. Liu, and A. Jia, "Assessment of gridded datasets of various near surface temperature variables over Heihe River Basin: Uncertainties, spatial heterogeneity and clear-sky bias," International Journal of Applied Earth Observation and Geoinformation, vol. 120, p. 103347, 2023/06/01/ 2023, doi: <https://doi.org/10.1016/j.jag.2023.103347>.